

# Adsorption of PTCDA on a partially KBr covered Ag(111) substrate

Ch Loppacher<sup>1,4</sup>, U Zerweck<sup>1</sup>, L M Eng<sup>1</sup>, S Gemming<sup>2</sup>, G Seifert<sup>2</sup>,  
C Olbrich<sup>3</sup>, K Morawetz<sup>3</sup> and M Schreiber<sup>3</sup>

<sup>1</sup> Institute of Applied Photophysics, TU Dresden, D-01062 Dresden, Germany

<sup>2</sup> Institute of Physical Chemistry and Electrochemistry, TU Dresden, D-01062 Dresden, Germany

<sup>3</sup> Institute of Physics, TU Chemnitz, D-09107 Chemnitz, Germany

E-mail: [Loppacher@iapp.de](mailto:Loppacher@iapp.de)

Received 28 November 2005, in final form 20 January 2006

Published 21 February 2006

Online at [stacks.iop.org/Nano/17/1568](http://stacks.iop.org/Nano/17/1568)

## Abstract

Ordered growth of 3,4,9,10-perylene-tetracarboxylic-dianhydride (PTCDA) on Ag(111) partially covered by one or two monolayers of KBr was investigated by non-contact AFM with molecular resolution. Different adsorption patterns are found on the pure substrate, the one covered by a single monolayer, and the one covered by two monolayers KBr. Simulations with an extended Ising-type model reproduce these experimental patterns very well. The adsorbate–adsorbate and the adsorbate–substrate interaction parameters obtained from the simulation are discussed with respect to the interactions at the Ag(111)|KBr interface. As a result, alkali halide covered metals can be used for tuning the interactions and designing adsorption systems, which opens up new possibilities in the control of self-assembled nanostructures.

## 1. Introduction

A major advantage of molecular electronics is the almost unlimited stock of organic molecules with a variety of tunable properties, which are sensitive to factors such as the intramolecular conformation, intermolecular interactions, or interface dipole formation with the surface of a metallic contact (for an overview on the metal/organic interface see e.g. [1–3]). The metal contact can provoke inactive layers. Thus, tunnelling-current induced luminescence was inhibited for planar molecules adsorbed on pure metals [4], but was detected for molecules with spacer legs [5], or molecules adsorbed on ultrathin oxide layers [6]. The importance of ultrathin insulation layers which decouple the molecule from its contact via a tiny tunnelling barrier has also been demonstrated by the enhanced charge carrier injection into organic devices on LiF-coated electrodes [7, 8] or on decanethiol self-assembled films [9].

For the *bottom-up* implementation of organic devices appropriate template surfaces are required, which do not influence the optical and electronic properties of the molecule

upon adsorption, and which facilitate an ordered growth. Insulating substrates might be ideal templates for organic growth. So far, ordered growth of organic films on pure insulators has been investigated by electron and x-ray diffraction methods ([10]; see section 3.2 in [1]). A few studies also used non-contact atomic force microscopy (nc-AFM) to investigate the ordering with molecular resolution (e.g. [11–14]). Although ultrathin alkali halide films on metal surfaces are promising surfaces and have been investigated in detail [15–19], so far only one study about selective adsorption of 3,10-di(propyl)perylene on striped patterns of CaF<sub>1</sub>/CaF<sub>2</sub> deposited onto the stepped semiconducting surface of Si(111) has been presented [20]. The fact that many weakly adsorbed organic thin films are oriented in relation with the substrate whereas upon larger coverage the orientation tends to be random indicates the delicate balance between adsorbate–adsorbate and adsorbate–substrate interactions.

From a theoretical point of view, several adsorption mechanisms have been proposed on the basis of electronic structure theory, ranging from weak van der Waals interactions between polarizable adsorbates and substrates to strong, even dissociative chemisorption accompanied with the formation of directed bonds [21–23]. The interaction of PTCDA with

<sup>4</sup> Author to whom any correspondence should be addressed.

metallic surfaces of Al [24], Ag [24, 25], Au [25], and with Ti [26] has been studied with first-principles electronic structure methods. The rather large distances between PTCDA and the M(111) (M = Al, Ag) surfaces of about 3 Å indicate an attractive interaction with a binding energy of about 1.2 eV per molecule [24]. Especially for PTCDA on Ag(111), this interaction is enhanced by a coupling of the vibrational modes of adsorbate and substrate, which is completely missing for PTCDA on Au(111); thus, the interaction in the latter system is considerably weaker [25]. In all cases, including Ti [26], metal-induced states in the gap of the organic molecule are formed, which influence the Schottky barrier height at the PTCDA-to-metal contact.

Here we present for the first time ordered growth of single monolayers (ML) of 3,4,9,10-perylene-tetracarboxylic-dianhydride (PTCDA) on a Ag(111) substrate partially covered by an ultrathin potassium bromide (KBr) film. Different adsorption patterns are observed on (I) pure Ag(111), (II) on 1 ML KBr|Ag(111), and (III) on 2 ML KBr|Ag(111) and rationalized by simulations with an extended Ising-type model [27].

## 2. Experimental details

All measurements were carried out at room temperature in an ultrahigh vacuum system (base pressure:  $>3 \times 10^{-8}$  mbar during sample preparation,  $>3 \times 10^{-10}$  mbar during measurements) with a scanning probe microscope operated in nc-AFM mode for topography imaging [28]. In this mode, two feedback controllers adjust the tip-sample distance and the excitation amplitude [29] in such a way that the frequency shift  $\Delta f$  and the oscillation amplitude are maintained constant<sup>5</sup>. For a few measurements, the local work function  $\phi$  was simultaneously detected by Kelvin probe force microscopy (KPFM) [30, 31]. This technique relies on a tip-sample bias-voltage modulation and reveals quantitative surface potential maps as recently shown for pure and KCl covered Au(111) surfaces [32].

The Ag(111) substrate was cleaned by repeated cycles of 1 keV Ar<sup>+</sup> ion sputtering and subsequent annealing to 720 K. After the last annealing cycle,  $\sim 1$  ML KBr was evaporated from a boron nitride crucible onto the Ag(111) surface during cool-down. The resulting surface shows a carpet-like growth of extended layers in the first KBr ML with quadratic islands in the second ML<sup>6</sup>. The bare substrate is still visible in a few

<sup>5</sup> The scanning probe microscope is a commercial cryogenic AFM/STM (Omicron NanoTechnology GmbH, D-65232 Taunusstein, Germany) which is equipped with an additional home-built vibration insulation. The instrument was operated in nc-AFM mode in which a microfabricated cantilever (spring constant  $k \sim 40$  N m<sup>-1</sup>) with a tip at the front end is excited at its bending eigenfrequency (levers used are NCL-type (long nc) cantilevers commercially available from NanoWorld AG, Rue Jaquet-Droz 1, CH-2007 Neuchâtel, Switzerland). The interaction between the oscillating tip and the surface changes the resonance frequency  $\Delta f$  with distance. The strong dependency of  $\Delta f$  on the tip-sample separation a few angstroms above the surface is used for topography feedback and provides high spatial resolution on all kinds of surfaces. The oscillation amplitude  $A_0$  is controlled by a second feedback loop. The power needed to keep a constant  $A_0$  is directly related to the tip-sample dissipation.

<sup>6</sup> *Carpet-like* describes the property of KBr films to grow connected across substrate steps; the substrate temperature and the evaporation rate have an influence on both the extension of connected areas as well as the size and number of the almost quadratic islands in the second ML. In our experiments the sample was kept at  $\sim 430$  K and the evaporation rate was 1 ML min<sup>-1</sup>.

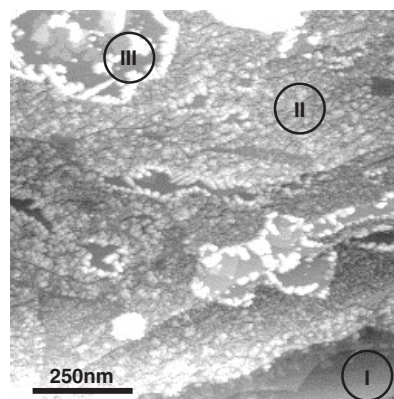


**Figure 1.** An nc-AFM topography image of PTCDA on KBr|Ag(111). Three different areas I, II, and III can be identified: (I) PTCDA on pure Ag(111) (lower right corner), (II) smaller PTCDA clusters on 1 ML KBr|Ag(111), and (III) larger clusters and planar growth of PTCDA on the quadratic islands in the second KBr ML (upper step edge);  $f_0 = 155.926$  kHz,  $k = 40$  N m<sup>-1</sup>,  $\Delta f = -34$  Hz,  $A_0 = 1.7$  nm.

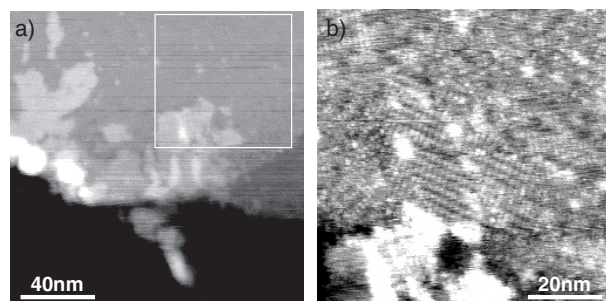


**Figure 2.** (a) Topography image of PTCDA adsorbed on pure Ag(111) close to a KBr covered area (not shown),  $f_0 = 155.926$  kHz,  $k = 40$  N m<sup>-1</sup>,  $\Delta f = -24$  Hz,  $A_0 = 1.7$  nm. (b) A close-up view inside the frame marked in (a) with molecular resolution shows partial ordering of PTCDA on Ag(111);  $\Delta f = -34$  Hz.

areas. KBr covered Ag(111) shows a decreased work function  $\phi$  by approximately 1 eV in comparison to pure Ag(111) independently on the KBr film thickness. Onto this partially KBr covered substrate, an additional 0.8 ML PTCDA was evaporated with the same deposition rate as for KBr and the sample kept at 300 K.

In the topography image (figure 1) we identify three different adsorption patterns: area I in the lower right corner where PTCDA grows partially ordered on pure Ag(111), area II with smaller, ordered and disordered PTCDA aggregates on the first KBr ML (figure 3(a)), and area III exhibiting large clusters and an ordered planar growth of PTCDA on areas which we assign to the typical quadratic islands of the second KBr ML.

### (I) PTCDA on pure Ag(111)

Figure 2(a) displays the growth of PTCDA on the pure Ag(111) surface. Close to KBr covered areas we observe a higher coverage of PTCDA indicating that the sticking coefficient is higher on Ag(111) than on KBr. Figure 2(b) was recorded inside the frame marked in figure 2(a) and displays partially ordered growth in the first PTCDA ML on Ag(111). The

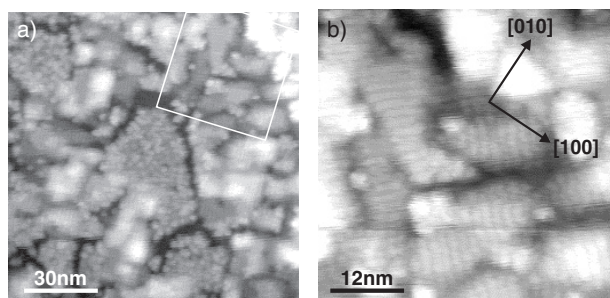


**Figure 3.** (a) Topography image of PTCDA on 1 ML KBr|Ag(111),  $f_0 = 155.926$  kHz,  $k = 40$  N m $^{-1}$ ,  $\Delta f = -32$  Hz,  $A_0 = 1.7$  nm, and (b) a close-up view inside the frame marked in (a),  $\Delta f = -35$  Hz. Two different aggregates are formed: one with disordered small clusters and one with molecular rods aligned  $\pm 45^\circ$  to the KBr [100] direction as indicated in the figure.

fact, that only partial ordering occurs might be due to a high number of defects in the Ag(111) substrate that possibly arise during KBr evaporation<sup>7</sup>. The distances and orientation in the molecular ordering, however, agree well with the almost rectangular unit cell (1.26 nm by 1.9 nm) of the herringbone structure described by Glöckler *et al* [33].

#### (II) PTCDA on 1 ML KBr|Ag(111)

On 1 ML KBr|Ag(111) we observe patterns with many small aggregates having a typical size of 2–6 nm in diameter and 0.4–0.8 nm in height as well as patterns with parallel rods that show a periodicity of  $\sim 1.6$  nm. A close-up view of the area marked in figure 3(a) reveals two perpendicular orientations of these rods that are aligned  $\pm 45^\circ$  with respect to the KBr [100] direction (figure 3(b)). Most probably, PTCDA molecules stack within these rods with the molecular plane perpendicular to the substrate. Rods of similar dimensions occur also for PTCDA on Au(100) evaporated on a cleaved KBr single crystal and exhibit the (010) plane of  $\alpha$ -PTCDA [34]. As in area I, these rods were not observed on the pure Au(100) single crystals, presumably due to the lack of impurities which serve as nucleation centres for the rod formation on the KBr-supported Au(100) films.

#### (III) PTCDA on 2 ML KBr|Ag(111)

Figure 4(a) shows the topography at a boundary between areas II (upper left corner) and III, which is parallel to the [010] direction of KBr. The larger clusters at the upper step edge on the second KBr ML are aligned  $\pm 45^\circ$  with respect to the KBr [100] direction, which again indicates ordered growth similar to the rods observed in area II. Far from step edges, planar growth aligned parallel to the KBr [100] direction is observed, as shown in figure 4(c) (topography) and 4(d) (dissipation) which display a close-up view of the frame marked in figure 4(a). On more extended terraces we expect these layers to form larger PTCDA crystals as observed on a cleaved single crystal KBr surface [13].

An interesting piece of information is revealed by the KPFM image in figure 4(b). The work function  $\phi$  of Ag(111)

<sup>7</sup> KBr might react with the Ag surface to form AgBr.

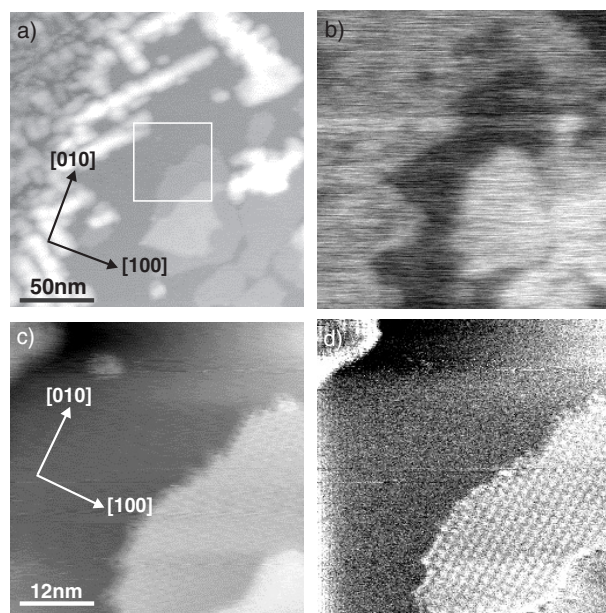


**Figure 4.** (a) Topography of PTCDA on 1 (upper left corner) and 2 ML KBr|Ag(111) recorded in the upper left corner of figure 1. The KPFM image in (b) shows three different contrasts:  $\phi$  is lowest on uncovered KBr|Ag(111), highest on planar PTCDA clusters on 2 ML KBr|Ag(111), and intermediate where PTCDA grows disordered or in rods. On 2 ML KBr|Ag(111) larger clusters form at the upper step edge and ordered growth of PTCDA is observed on larger terraces. A close-up view as depicted by the frame in (a) shows images with molecular resolution in topography (c) and dissipation (d). The arrows indicate the crystallographic orientation of the KBr film.

is reduced by  $\sim 1$  eV on KBr covered areas (darkest contrast in figure 4(b)). Evaporation of PTCDA onto these KBr layers surprisingly increases  $\phi$  again by  $\sim 0.2$  eV on 2 ML KBr when the molecules show planar growth (brightest areas in figure 4(b)), and by 0.1 eV in all other areas where PTCDA grows in rods or unordered clusters, independent whether the molecules are adsorbed on the first or the second ML. The astonishing result in our experiments is the fact that different adsorption patterns are obtained on areas II and III. One reason for that might be the interface dipole formation between Ag(111) and KBr. Earlier KPFM experiments have shown that this dipole is confined to the first ML only [19]. Hence, we expect a different interaction between PTCDA and the substrate on area II compared to area III concerning the charge distribution or the adsorption geometry, or both. Indeed, the KPFM image in figure 4(b) shows larger contrast for PTCDA molecules adsorbed in a planar geometry on KBr|Ag(111) than for all other patterns independent of whether the KBr film underneath has a thickness of 1 or 2 ML. A second explanation is the formation of weak bonds between silver atoms and the bromine ion in the first KBr ML. We favour the second explanation because similar adsorption patterns are formed on KBr covered Cu(111) substrates. A different situation is encountered for the less reactive metal Au: on KBr|Au(111) substrates PTCDA forms several ML high single crystals, which nucleate along step edges very similar to cleaved KBr single crystal surfaces [13].

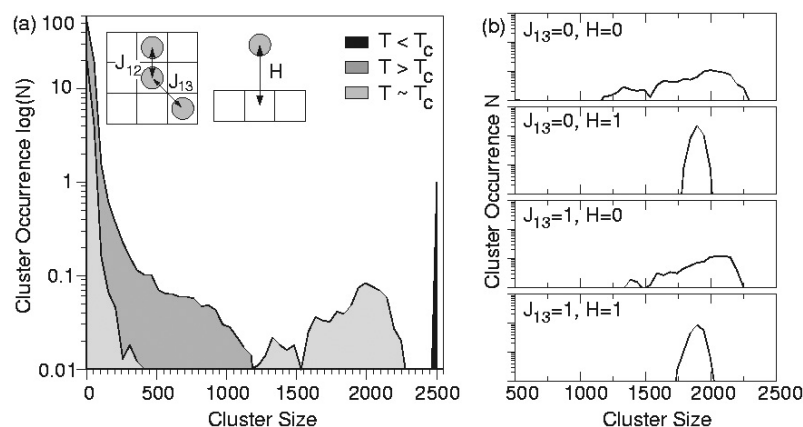


**Figure 5.** (a) Cluster size distribution for the classical Ising model at three different temperatures. The area shaded in dark grey denotes the cluster size distribution at  $T = 2T_c$ , the area shaded in light grey is obtained at  $T = T_c$ , and the black shaded curve corresponds to a low temperature of  $T = 0.1T_c$ . The inset visualizes the lateral and vertical interaction terms. At  $T = T_c$  the system is most sensitive to changes of the interaction parameters. Thus, panel (b) depicts four standard cluster size distributions for different values of lateral interaction  $J$  and vertical interaction  $H$  at  $T = T_c$ .

### 3. Simulation

The experimental observation of three different adsorption patterns on the three substrate areas suggests that different interaction strengths and probably also adsorption mechanisms are encountered for PTCDA on Ag(111), on 1 ML KBr|Ag(111), or on 2 ML KBr|Ag(111). Unfortunately, suitable model systems including several PTCDA molecules on the different surfaces are too large to be thoroughly investigated on a fully first-principles basis. Thus, a mesoscopic approach, based on first-principles parameters, was employed here to rationalize the interplay between the PTCDA–substrate interaction and the lateral, intermolecular interaction between neighbouring PTCDA molecules. As described in more detail in the appendix, an extended Ising Hamiltonian was employed, whose parameters were derived from first-principles calculations on the interaction strength of PTCDA dimers and of single, adsorbed PTCDA molecules. The influence of temperature-induced adsorption, desorption, and surface diffusion processes was accounted for by a Metropolis Monte Carlo algorithm.

Originally this model was developed to study the temperature dependence of the interaction between spins  $s_i$  via a coupling constant  $J_{12}$  in an external magnetic field  $H$ . It has been transferred successfully to the structure and phase stability of both weakly [35] and strongly [36] bound adsorbates on planar metal surfaces, as well as self-assembly processes on semiconductors [37]. In our extended version the nearest and next-nearest neighbour interactions between adsorbed molecules were included as coupling constants  $J_{12}$  and  $J_{13}$ , the on-site term  $H$  represents the interaction with the substrate, and the site occupancy takes the role of the spin.

The value of  $J_{12} = J_{13} = J$  was derived from first-principles calculations on PTCDA dimers [38, 39], and the adsorption energy  $H$  was varied within the bounds suggested by first-principles calculations of the interaction of PTCDA and Al(111) [24], Ag(111) [24, 25], Au(111) [25], and Ti [26]. For each set of parameters ( $H, J$ ) the system exhibits an order–disorder transition at a critical temperature  $T_c$ , which

increases with increasing values of  $J$  and  $H$  and leads to the temperature-dependent cluster size distribution depicted in figure 5, left panel<sup>8</sup>. At a low temperature of  $T \approx 0.1T_c$  one big cluster covers the whole substrate (figure 5(a), area shaded in black), whereas at  $T \approx 2T_c$  monomers or small clusters are obtained (figure 5(a), area shaded in dark grey). Only close to  $T_c$  are intermediate cluster sizes observed (figure 5(a), area shaded in light grey); thus  $T \approx T_c$  is the most promising temperature for tuning the self-assembly properties.

Figure 5(b) displays the changes of the cluster size distribution, when  $J_{13}$  and  $H$  are successively added to the standard Ising model (figure 5(b), top curve). The most prominent change occurred when only the vertical interaction was added ( $H = J_{12}$ ):  $T_c$  increases from the classical value of  $2.32 k_B^{-1}$  to  $5.28 k_B^{-1}$  and a unimodal distribution with a considerably reduced width is obtained, whose centre of mass shifts to slightly larger cluster sizes (figure 5(b), second from top). If only the lateral interactions  $J_{13}$  ( $=J_{12}$ ) are added to the standard Ising Hamiltonian,  $T_c$  also increases to  $5.64 k_B^{-1}$ , the distribution is still bimodal, but the maximum shifts to larger cluster sizes and the distribution width  $w$  decreases by 2%, which reflects denser and more ordered packing (figure 5(b), second from bottom). If both ordering factors  $J_{13}$  and  $H$  are included in the simulation (figure 5(b), bottom curve), the cluster size distribution again exhibits one maximum and seems to be dominated by the vertical interaction  $H$ . However, the distribution width including lateral interactions is larger than the one obtained with  $J_{13} = 0$  and the maximum is shifted to smaller cluster sizes. This finding may seem unexpected at first glance, but it reflects the competition between the two different ordering factors  $J_{13}$  and  $H$ . The maximum cluster sizes are indeed reached if both  $J_{13}$  and  $H$  are included in the simulation; however, only as a statistically rare event. It is by far outnumbered by the cases in which the vertical interaction  $H$

<sup>8</sup> The cluster sizes at the critical temperature were evaluated with the help of the Hoshen–Kopelman cluster recognition algorithm, and the cluster size distribution statistics was determined from averaging over at least  $1 \times 10^6$  Monte Carlo steps, which corresponds to at least 400 spin flips per site.

pins many cluster nucleation sites, and both  $J_{12}$  and  $J_{13}$  assist the growth of smaller clusters from these seeds.

#### 4. Conclusion

Our model simulation with fixed lateral interactions  $J_{12} = J_{13}$  could nicely reproduce the experimentally observed cluster formation by varying the vertical adsorbate–substrate interaction  $H$  as the substrate changes from Ag(111) (area I) to 1 ML KBr|Ag(111) (area II) and to 2 ML KBr|Ag(111) (area III). The following three characteristic adsorption regimes can be discriminated.

- (i) Area I, where  $H$  is the dominant interaction ( $H \gg J$ ).
- (ii) Area III, where  $J_{12}$  and  $J_{13}$  are the dominant interactions ( $J \gg H$ ).
- (iii) Area II, where  $J_{12}$ ,  $J_{13}$ , and  $H$  are competing ( $H \approx J$ ).

For the areas I and III the AFM images exhibit large and regular clusters in accordance with the simulated cluster size distribution obtained when one interaction dominates the others. The Monte-Carlo-Ising simulations also reproduce the experimental occurrence of many smaller assemblies in the intermediate region II. In that case, a competition of different cluster stabilization mechanisms leads to the pinning of many smaller clusters. Choosing an appropriate combination of alkali halide films and metal substrate provides an excellent possibility to influence this competition and to create model systems to evaluate theoretical models. Therefore, we propose alkali halide covered metal for tuning the interactions and designing adsorption systems on which the structuring of large surface areas with nanometre resolution becomes possible.

#### Acknowledgments

Financial support from the German Science Foundation under grant Nos SFB 287 and SPP 1157 is gratefully acknowledged. We thank T Fritz (TU Dresden), R Scholz (TU Chemnitz), and H Emmerich (RWTH Aachen) for discussion and advice.

#### Appendix

An extended Ising-type model has been developed to study the coverage and the pattern evolution of adsorbate clusters at planar and stepped surfaces by Monte Carlo simulations. The standard Ising model was developed to describe the temperature and magnetic-field dependence of the magnetic properties of a spin system with spin values  $s_i = +1$  or  $-1$ , an inter-spin coupling constant  $J_{12}$  between neighbouring sites, and an external magnetic field  $H$ . The total energy of the system is given by the following Hamiltonian:

$$E_{\text{tot}} = \sum_i \left[ \sum_j J_{12} s_i s_j + H s_i \right], \quad (\text{A.1})$$

where the sum  $\sum_j$  runs over the  $j$  nearest neighbours of site  $i$ , and  $\sum_i$  sums over all sites. Below a critical temperature,  $T_c$ , all spins are ordered and a net magnetization can occur in the standard two-dimensional Ising model; at  $T_c$  an order–disorder phase transition takes place, and above  $T_c$  the random distribution of the spins leads to a net magnetization of zero.

Without an external magnetic field  $H$  the transition is of second order, otherwise it is of first order [27, 40–42]. In our new model the influence factors for the adsorption of molecules on surfaces are mapped onto this Ising model in the following way: the spin  $s_i$  denotes the site occupancy with  $s_i = 1$  for occupied and  $s_i = -1$  for unoccupied sites. The coupling constant  $J_{12}$  represents the lateral adsorbate–adsorbate interaction, and the vertical adsorbate–substrate interaction is mapped to the magnetic field  $H$ . In order to model more realistic adsorption systems, the Hamiltonian was augmented by diagonal interaction terms  $J_{13}$  to the next-nearest neighbouring molecules which account for the more complex and long-range lateral interactions in organic films caused by anisotropies of the molecules. Hence, the modified Hamiltonian is given by

$$E_{\text{tot}} = \sum_i \left[ \sum_j J_{12} s_i s_j + H s_i \right] + \sum_i \left[ \sum_k J_{13} s_i s_k \right], \quad (\text{A.2})$$

where  $i$  runs over all sites,  $j$  runs over the nearest neighbours of site  $i$ , and  $k$  runs over the next-nearest neighbours.

#### References

- [1] Forrest S R 1997 *Chem. Rev.* **97** 1793
- [2] Cahen D and Kahn A 2003 *Adv. Mater.* **15** 271
- [3] Barlow S M and Raval R 2003 *Surf. Sci. Rep.* **50** 201
- [4] Hoffmann G, Libioulle L and Berndt R 2002 *Phys. Rev. B* **65** 212107
- [5] Fujita D *et al* 2000 *Surf. Sci.* **454–456** 1021
- [6] Qiu X H, Nazin G V and Ho W 2003 *Science* **299** 542
- [7] Mori T, Fujikawa H, Tokito S and Taga Y 1998 *Appl. Phys. Lett.* **73** 2763
- [8] Schlaf R *et al* 1998 *J. Appl. Phys.* **84** 6729
- [9] Gerstenberg M C *et al* 2000 *Phys. Rev. B* **61** 7678
- [10] Möbius M, Karl N and Kobayashi T 1992 *J. Cryst. Growth* **116** 495
- [11] Nony L *et al* 2004 *Nano Lett.* **4** 2185
- [12] Burke S A, Mativetsky J M, Hoffmann R and Grütter P 2005 *Phys. Rev. Lett.* **94** 096102
- [13] Kunstmann T *et al* 2005 *Phys. Rev. B* **71** 121403(R)
- [14] Yamada H *et al* 2002 *Appl. Surf. Sci.* **188** 391
- [15] Hebenstreit W *et al* 2000 *Phys. Rev. Lett.* **85** 5376
- [16] Bennewitz R *et al* 2000 *Phys. Rev. B* **62** 2074
- [17] Repp J, Fölsch S, Meyer G and Rieder K-H 2001 *Phys. Rev. Lett.* **86** 252
- [18] Kiguchi M *et al* 2003 *Phys. Rev. Lett.* **90** 196803
- [19] Loppacher C, Zerweck U and Eng L M 2004 *Nanotechnology* **15** S9
- [20] Rauscher H *et al* 1999 *Chem. Phys. Lett.* **303** 363
- [21] Rösch N *et al* 2004 *Theor. Comput. Chem.* **15** 367
- [22] Kroes G J *et al* 2002 *Acc. Chem. Res.* **35** 193
- [23] Tully J C 2000 *Ann. Rev. Phys. Chem.* **51** 153
- [24] Picozzi S *et al* 2003 *Phys. Rev. B* **68** 195309
- [25] Eremtchenko M, Bauer D, Schaefer J A and Tautz F S 2004 *New. J. Phys.* **6** 4
- [26] Palma A, Pasquarello A and Car R 2002 *Phys. Rev. B* **65** 155314
- [27] Morawetz K, Olbrich C, Gemming S and Schreiber M 2005 in preparation
- [28] Martin Y, Williams C C and Wickramasinghe H K 1987 *J. Appl. Phys.* **61** 4723
- [29] Loppacher C *et al* 2000 *Phys. Rev. B* **62** 13674
- [30] Nonnenmacher M, O’Boyle M P and Wickramasinghe H K 1991 *Appl. Phys. Lett.* **58** 2921
- [31] Weaver J M R and Abraham D W 1991 *J. Vac. Sci. Technol. B* **9** 1559
- [32] Zerweck U *et al* 2005 *Phys. Rev. B* **71** 125424

- 
- [33] Glöckler K *et al* 1998 *Surf. Sci.* **405** 1
- [34] Schmitz-Hübsch T *et al* 1999 *Surf. Sci.* **437** 163
- [35] Alfè D and Baroni S 1997 *Surf. Sci.* **382** L666
- [36] Ocko B M, Wang J X and Wandlowski T 1997 *Phys. Rev. Lett.* **79** 1511–4
- [37] LaBella V P *et al* 2001 *J. Vac. Sci. Technol. B* **19** 1640
- [38] Vragovic I, Scholz R and Schreiber M 2002 *Europhys. Lett.* **57** 228
- [39] Vragovic I and Scholz R 2003 *Phys. Rev. B* **68** 155202
- [40] Onsager L 1944 *Phys. Rev.* **85** 117
- [41] Yang C N 1952 *Phys. Rev.* **85** 808
- [42] Domb C and Sykes P 1957 *Proc. R. Soc. A* **240** 214